Chapter 1

Data Analysis

Update the int. lumi. everywhere.

The signature of GGM SUSY particle production in this search is an excess of two-photon events with high $\not\!\!E_T$. $\not\!\!E_T$ is reconstructed using the particle flow algorithm as described in Sec. **??**. Candidate two-photon events, as well as control events, are selected according to the offline object criteria presented in Secs. **??** and **??**, the event quality criteria in Sec. **??**, and the trigger requirements in Sec. **??**. These are summarized in Table 1.1.

This search utilizes 4.7 fb^{-1} of CMS data collected during the period April-December 2011, corresponding to the following datasets [**?**]:

- `/Photon/Run2011A-05Jul2011ReReco-ECAL-v1/AOD`
- `/Photon/Run2011A-05Aug2011-v1/AOD`
- `/Photon/Run2011A-03Oct2011-v1/AOD`
- `/Photon/Run2011B-PromptReco-v1/AOD`

The search strategy is to model the backgrounds to the GGM SUSY signal using $\not\!\!E_T$ shape templates derived from the control samples, and then to look for a high-$\not\!\!E_T$

excess above the estimated background in the $\gamma\gamma$ sample. There are two categories of backgrounds: QCD processes with no real $\not\!\!E_T$ and electroweak processes with real $\not\!\!E_T$ from neutrinos. The relevant QCD background processes are multijet production with at least two jets faking photons, photon + jet production with at least one jet faking a photon, diphoton production, and Z production with a radiated photon where at least one of the Z decay products (typically a jet) fakes a photon. The relevant electroweak background processes, which are small compared to the QCD background, involve $W \to e\nu$ decay with a recoiling jet that fakes a photon or a real radiated photon (the W may come from the decay of a top quark in $t\bar{t}$ events). In both cases, the electron is misidentified as a photon due to a small inefficiency in reconstructing the electron pixel seed. The main diagrams contributing to the QCD(electroweak) backgrounds are shown in Figure **??**(**??**). **Generate these Feynman diagrams.**

Figure **??** shows the $\not\!\!E_T$ spectrum of the $\gamma\gamma$ search data sample overlaid on the $\not\!\!E_T$ spectra of MC simulated background components. The MC spectra are normalized to the integrated luminosity of the $\gamma\gamma$ data sample. **Make this plot.** The dominant background components are QCD inclusive photon processes. The MC is not used in the actual background estimation. It is just shown here to illustrate the breakdown of backgrounds.

Data control samples are used to model all of the backgrounds. The primary control sample used to model the QCD background is the ff sample, which is similar to the candidate $\gamma\gamma$ sample but with combined isolation or $\sigma_{i\eta i\eta}$ cuts inverted. The cuts on these variables are used to distinguish between photons and jets, so by inverting those cuts, the resulting ff sample becomes enriched with QCD dijets. Because the fake photons are still required to pass a tight cut on H/E, they are guaranteed to be very electromagnetic jets, with an EM energy scale and resolution similar to that of the candidate photons. This insures that the resulting estimate of the $\not\!\!E_T$ shape does not have too long of a tail from severe HCAL mis-measurements that are actually

rare in the $\gamma\gamma$ sample, as shown in Figure **??**. **Plot the $\gamma\gamma/ff$ $\not\!\!E_T$ agreement for different values of the ff H/E cut in MC. Make the same plot in data for a restricted $\not\!\!E_T$ range?**

As a cross-check, the ee sample is also used to model the QCD background. This sample of Z decays should have no true $\not\!\!E_T$, just like the ff sample, and the electron definition (differing from the photon definition only in the presence of a pixel seed) insures that the electron energy scale and resolution is similar to that of the photon.

Finally, the $e\gamma$ sample is used to model the electroweak background from $W \to e\nu$ decays. The $e\gamma$ $\not\!\!E_T$ distribution is scaled by the electron→photon misidentification rate to predict the number of $W\gamma$, W + jet, and $t\bar{t}$ events in the $\gamma\gamma$ sample.

The remainder of this chapter describes the data analysis procedures and the final results of the search. Sec. 1.1 addresses the QCD background estimation. Sec. **??** addresses the electroweak background estimation. The chapter concludes with a discussion of systematic errors in Sec. 1.3 and a presentation of the final results in Sec. 1.4.

1.1 Modeling the QCD Background

1.1.1 Outline of the Procedure

Due to the fact that the CMS ECAL energy resolution is much better than the HCAL energy resolution, the energies of the two candidate photons in the events of the $\gamma\gamma$ sample are typically measured to far greater accuracy and precision than the energy of the hadronic recoil in those events. Therefore, fake $\not\!\!E_T$ in the $\gamma\gamma$ sample is almost entirely the result of hadronic mis-measurement in QCD dijet, photon + jet, and diphoton events. The strategy employed to model this background is to find a control sample in data consisting of two well-measured EM objects, just like the candidate $\gamma\gamma$ sample, and assign each event a weight to account for the underlying

kinematic differences between the control and candidate samples. Once the reweighted $\not\!\!E_T$ spectrum of the control sample is created, it is then normalized in the low-$\not\!\!E_T$ region, the assumption being that GGM SUSY does not predict a significant amount of events at low $\not\!\!E_T$. There are three aspects to this QCD background estimation procedure that bear highlighting:

Choice of control sample Since the underlying cause of $\not\!\!E_T$ in the candidate sample is mis-measured hadronic activity, a control sample with similar hadronic activity to the candidate sample should be chosen. Hadronic activity refers to number of jets, jet E_T, pileup, etc.

Reweighting The control sample is reweighted so that its $\not\!\!E_T$ spectrum appears as it would if the control sample had the same kinematic properties as the candidate sample (i.e. particle p_T and η distributions, etc.). By choosing an appropriate control sample and reweighting it, the control $\not\!\!E_T$ distribution should now match both the hadronic activity and the kinematics of the candidate sample.

Normalization Finally, the control $\not\!\!E_T$ distribution is normalized in a region of low $\not\!\!E_T$, where contamination from the expected GGM SUSY signal is small. This implies an extrapolation of the low-$\not\!\!E_T$ QCD background prediction to the high-$\not\!\!E_T$ signal region.

As explained in the beginning of this chapter, the *ff* sample is used as the primary QCD control sample, while the *ee* sample is used as a cross-check. Both samples have two well-measured EM objects per event, no real $\not\!\!E_T$, and similar hadronic activity to the $\gamma\gamma$ sample. Figure 1.1 shows a comparison of the shapes of some distributions relevant to hadronic activity between the $\gamma\gamma$, *ee*, and *ff* samples. In general, the *ee* sample has less hadronic activity than the $\gamma\gamma$ and *ff* samples, as shown by the more steeply falling *ee* distributions in Figs. 1.1a, 1.1b, 1.1c, and 1.1d. In addition to the

kinematic reweighting, there is also a reweighting by number of jets per event, which attempts to correct for this difference (see Sec. 1.1.2).

1.1.2 Reweighting

To reweight the control sample events to match the kinematics of the candidate sample events, a weight based on the p_T of the di-EM-object system and the number of jets in the event is used. As explained in Sec. 1.1.1, $\not\!\!E_T$ in the $\gamma\gamma$, ff, and ee samples is due to the poorly measured hadronic recoil off the well-measured di-EM system. Therefore, the p_T of the di-EM system is a good handle on the true magnitude of the hadronic recoil, which affects the measured $\not\!\!E_T$. The di-EM system is depicted in Figure 1.2.

Whereas the di-EM p_T reweighting accounts for differences in production kinematics between the control and $\gamma\gamma$ samples, a simultaneous reweighting based on the number of jets in the event accounts for differences in hadronic activity between the samples, especially between ee and $\gamma\gamma$ (cf. Fig. 1.1). Jets are defined as in Table **??**. Figure 1.3 shows the effect of reweighting by number of jets per event, which is to increase(decrease) the tail of the $ee(ff)$ $\not\!\!E_T$ spectrum.

Although the electron and photon energies are well measured by the ECAL, the ECAL-only measurement of the fake photon energy (cf. Sec **??**) is biased slightly low due to the fact that fakes (which are really jets) tend to deposit some energy in the HCAL. This can be seen in Figs. 1.4 and 1.5, which show the relative difference between the ECAL-only E_T measurement and the PF E_T measurement vs. EMF for electrons, photons, and fakes. PF E_T is defined as the `L1Fast`-corrected E_T of the nearest PF jet with $p_T \geq 20$ GeV (i.e., the E_T of the PF jet object reconstructed from the same ECAL shower as the fake photon). On average, the fakes tend to deposit a few percent more energy in the HCAL than the electrons or photons, which is recovered by the PF algorithm. For this reason, the PF p_T is used in the calculation

Table 1.1: Selection criteria for $\gamma\gamma$, $e\gamma$, ee, and ff events.

Variable	Cut			
	$\gamma\gamma$	$e\gamma$	ee	ff
HLT match	IsoVL	IsoVL	IsoVL	IsoVL || R9Id
E_T	$> 40/$ > 25 GeV	$> 40/$ > 25 GeV	$> 40/$ > 25 GeV	$> 40/$ > 25 GeV
SC $\lvert\eta\rvert$	< 1.4442	< 1.4442	< 1.4442	< 1.4442
H/E	< 0.05	< 0.05	< 0.05	< 0.05
$R9$	< 1	< 1	< 1	< 1
Pixel seed	No/No	Yes/No	Yes/Yes	No/No
I_{comb}, $\sigma_{i\eta i\eta}$	< 6 GeV && < 0.011	< 6 GeV && < 0.011	< 6 GeV && < 0.011	< 20 GeV && (≥ 6 GeV || ≥ 0.011)
JSON	Yes	Yes	Yes	Yes
No. good PVs	≥ 1	≥ 1	≥ 1	≥ 1
ΔR_{EM}	> 0.6	> 0.6	> 0.6	> 0.6
$\Delta\phi_{\text{EM}}$	≥ 0.05	≥ 0.05	≥ 0.05	≥ 0.05

Table 1.2: Definition of HB/HE/HF hadronic jets. **Add a footnote describing the PF electron and PF muon definitions, with references.**

Variable	Cut
Algorithm	`L1FastL2L3Residual` corrected PF (cf. Sec. **??**)
p_T	> 30 GeV
$\lvert\eta\rvert$	< 5.0
Neutral hadronic energy fraction	< 0.99
Neutral electromagnetic energy fraction	< 0.99
Number of constituents	> 1
Charged hadronic energy	> 0.0 GeV if $\lvert\eta\rvert < 2.4$
Number of charged hadrons	> 0 if $\lvert\eta\rvert < 2.4$
Charged electromagnetic energy fraction	< 0.99 if $\lvert\eta\rvert < 2.4$
ΔR to nearest electron, muon, or one of the two primary EM objects	> 0.5

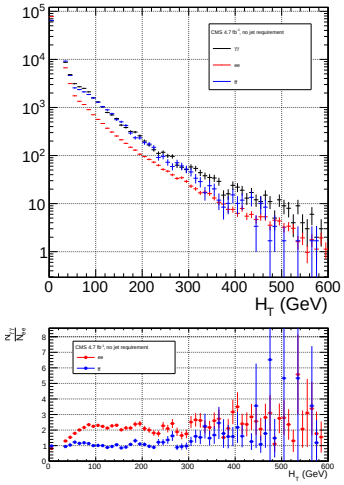

(a) H_T, defined as the scalar sum of corrected jet E_T for jets defined as in Table 1.2.

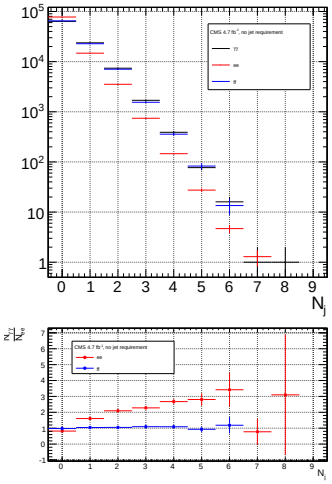

(b) Number of jets per event for jets defined as in Table 1.2.

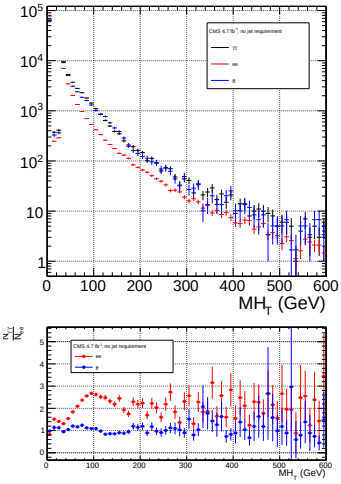

(c) $\not{H}_T$, defined as the magnitude of the negative vectorial sum of corrected jet E_T for jets defined as in Table 1.2.

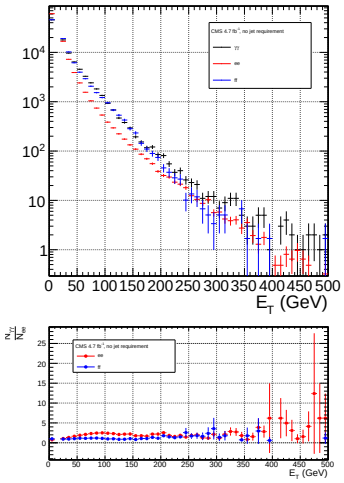

(d) Corrected E_T for the jet with the largest corrected E_T per event, for jets defined as in Table 1.2 (excluding the p_T requirement).

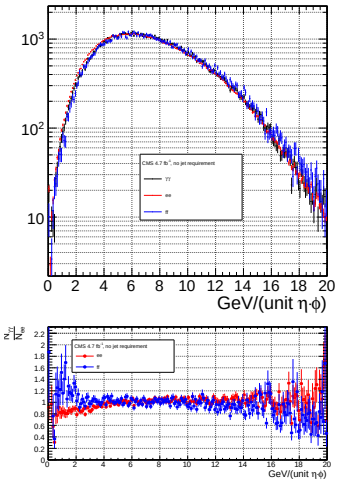

(e) ρ (average pileup energy density in the calorimeters per unit $\eta \cdot \phi$, cf. Sec. **??**).

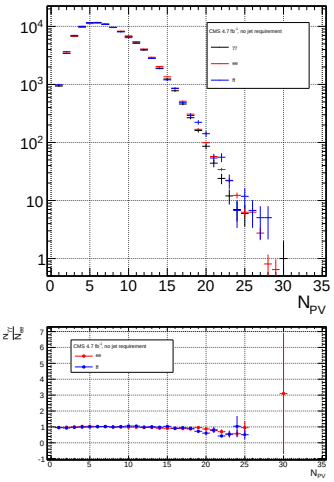

(f) Number of good reconstructed primary vertices per event according to the criteria of Sec. **??**.

Figure 1.1: Comparison of the shapes of some distributions relevant to hadronic activity between the $\gamma\gamma$, ee (81 GeV $\leq m_{ee} <$ 101 GeV), and $\not{f}\not{f}$ samples. The ee and $\not{f}\not{f}$ distributions are normalized to the number of events in the $\gamma\gamma$ distribution. Errors are statistical only.

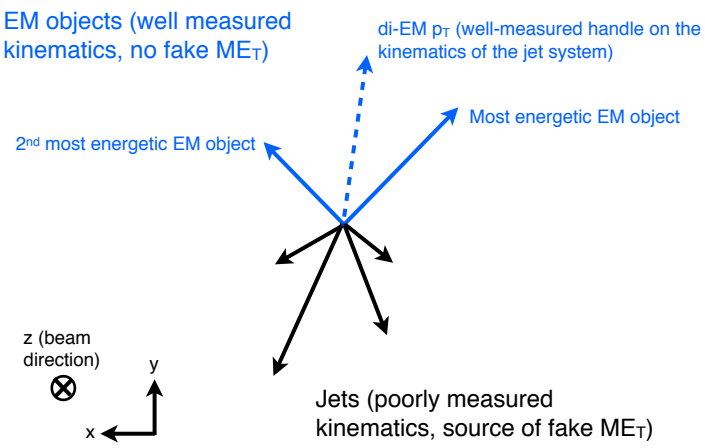

Figure 1.2: Cartoon showing the di-EM system in blue and the hadronic recoil in black. The di-EM p_T (dashed blue line) is used to reweight the control sample kinematic properties to match those of the candidate $\gamma\gamma$ sample.

.

of di-EM p_T rather than the ECAL-only p_T.[1] This leads to a modest improvement in the agreement between the *ee* and *ff* $\not\!\!E_T$ spectra, as shown in Figure 1.6.

The control sample event weights are defined as

$$w_{ij} = \frac{N_{\text{control}}}{N_{\gamma\gamma}} \frac{N^{ij}_{\gamma\gamma}}{N^{ij}_{\text{control}}} \tag{1.1}$$

where i runs over the number of di-EM p_T bins, j runs over the number of jet bins, N_{control} is the total number of events in the control sample, $N_{\gamma\gamma}$ is the total number of events in the $\gamma\gamma$ sample, $N^{ij}_{\gamma\gamma}$ is the number of $\gamma\gamma$ events in the i^{th} di-EM p_T bin and j^{th} jet bin, and N^{ij}_{control} is the number of control sample events in the i^{th} di-EM p_T bin and j^{th} jet bin. The effect of the reweighting is more significant for the *ee* sample than for the *ff* sample, as shown in Figure 1.7.

The *ee* sample contains a non-negligible background of $t\bar{t}$ events in which both W bosons decay to electrons. These events have significant real $\not\!\!E_T$ from the two

[1] In the few events ($\mathcal{O}(10^{-3})$) in which two PF jet objects, corresponding to the two electrons or fakes, are not found, the ECAL-only p_T is used.

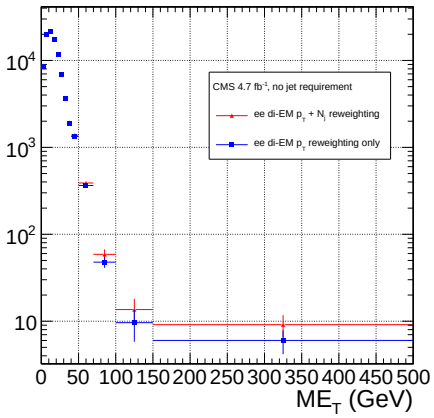

(a) ee $\not\!\!E_T$ spectra.

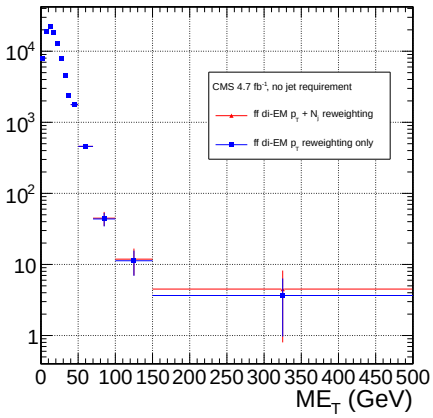

(b) ff $\not\!\!E_T$ spectra.

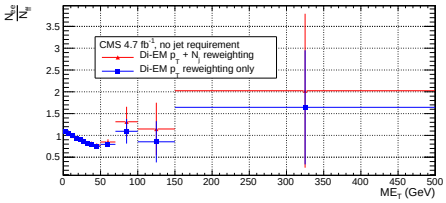

(c) Ratio of ee to ff $\not\!\!E_T$ spectra.

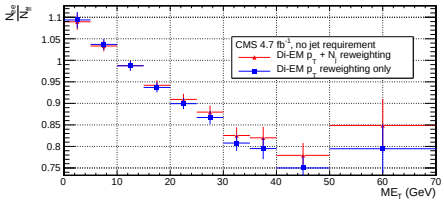

(d) Ratio of ee to ff $\not\!\!E_T$ spectra, zoomed x-axis.

Figure 1.3: $\not\!\!E_T$ spectra of the reweighted ee (81 GeV $\leq m_{\mathrm{ee}} <$ 101 GeV) and ff control samples. Blue squares indicate di-EM p_T reweighting only; red triangles indicate di-EM p_T + number of jets reweighting. PF p_T (cf. p. 10) is used to calculate the di-EM p_T. The full normalization procedure is employed, along with ee sideband subtraction (discussed in at the end of this section). Error bars include statistical, reweighting, and normalization error (see Sec. 1.3).

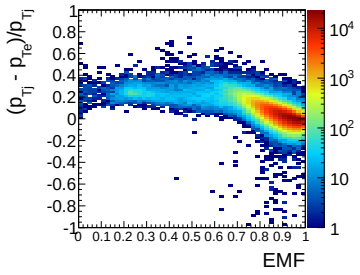

(a) Leading electron in ee events.

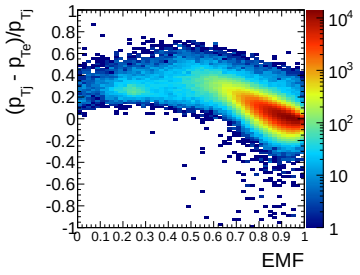

(b) Trailing electron in ee events.

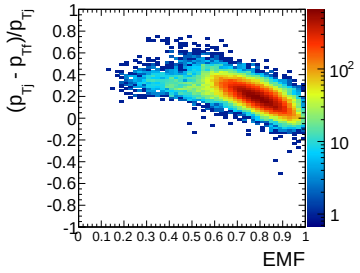

(c) Leading fake in ff events.

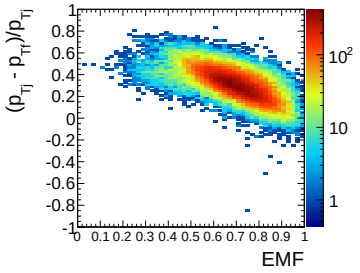

(d) Trailing fake in ff events.

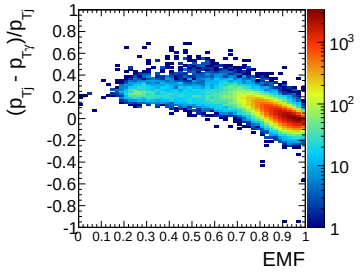

(e) Leading photon in $\gamma\gamma$ events.

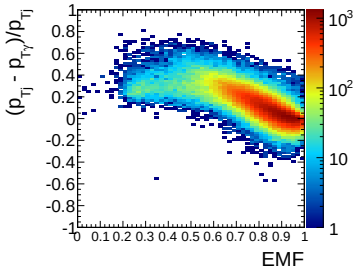

(f) Trailing photon in $\gamma\gamma$ events.

Figure 1.4: Relative difference between the ECAL-only E_T measurement and the PF E_T measurement vs. EMF. PF E_T is defined in the text.

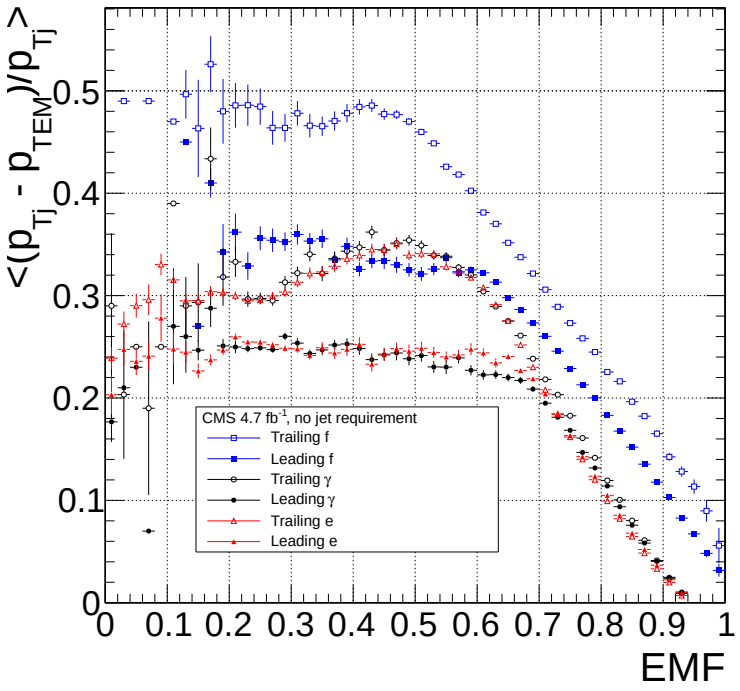

Figure 1.5: Average relative difference between the ECAL-only E_T measurement and the PF E_T measurement vs. EMF for the leading (filled marker) and trailing (open marker) electrons in ee events (red triangles), fakes in ff events (blue squares), and photons in $\gamma\gamma$ events (black circles). These are nothing more than profile histograms of Fig. 1.4. PF E_T is defined in the text. Error bars are statistical only.

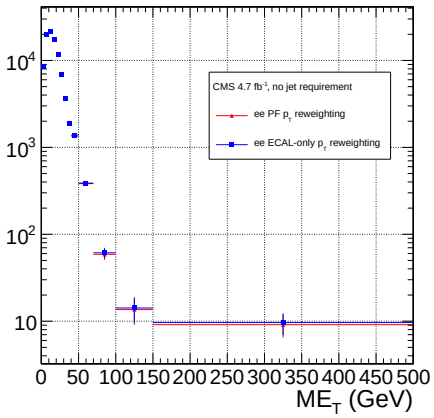

(a) ee $\not\!\!E_T$ spectra.

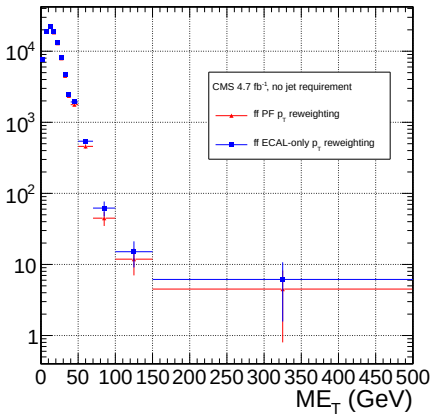

(b) ff $\not\!\!E_T$ spectra.

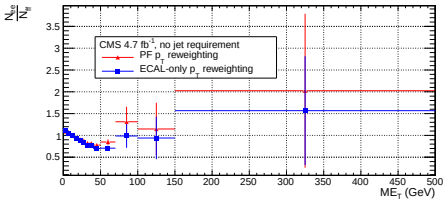

(c) Ratio of ee to ff $\not\!\!E_T$ spectra.

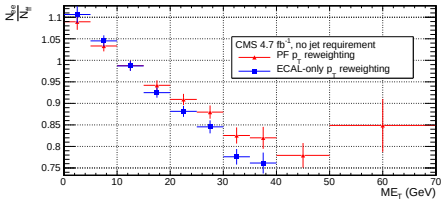

(d) Ratio of ee to ff $\not\!\!E_T$ spectra, zoomed x-axis.

Figure 1.6: $\not\!\!E_T$ spectra of the reweighted ee (81 GeV $\leq m_{\mathrm{ee}} <$ 101 GeV) and ff control samples. Blue squares indicate reweighting using the ECAL-only p_T estimate; red triangles indicate reweighting using the PF p_T estimate. The full reweighting and normalization procedure is employed, along with ee sideband subtraction (discussed at the end of this section). Error bars include statistical, reweighting, and normalization error (see Sec. 1.3).

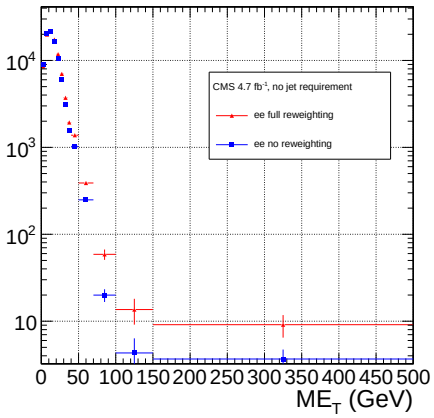

(a) ee $\not\!\!E_T$ spectra.

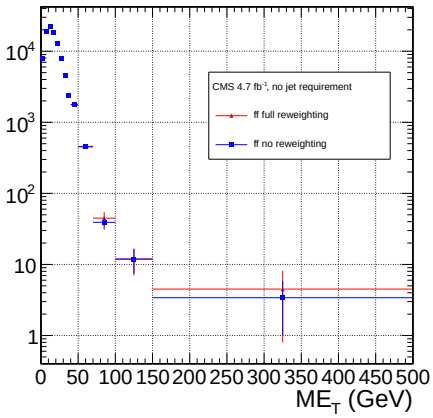

(b) ff $\not\!\!E_T$ spectra.

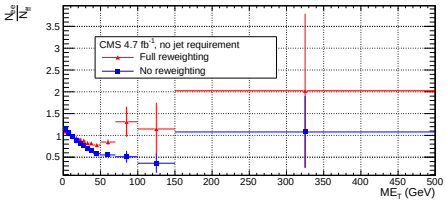

(c) Ratio of ee to ff $\not\!\!E_T$ spectra.

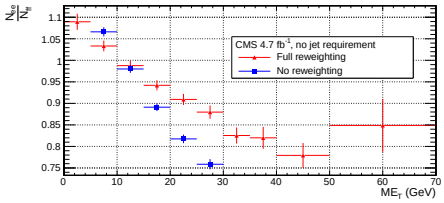

(d) Ratio of ee to ff $\not\!\!E_T$ spectra, zoomed x-axis.

Figure 1.7: $\not\!\!E_T$ spectra of the ee (81 GeV $\leq m_{\text{ee}} <$ 101 GeV) and ff control samples. Red triangles indicate full di-EM p_T + number of jets reweighting; blue squares indicate no reweighting. PF p_T (cf. p. 10) is used to calculate the di-EM p_T. The full normalization procedure is employed, along with ee sideband subtraction (discussed at the end of this section). Error bars include statistical, reweighting (where appropriate), and normalization error (see Sec. 1.3).

neutrinos (unlike the $\gamma\gamma$ events), and therefore inflate the background estimate at high $\not\!\!E_T$. In order to remove the $t\bar{t}$ contribution from the ee sample, a sideband subtraction method is employed.

Only events in the ee sample with 81 GeV $\leq m_{\rm ee} <$ 101 GeV, where $m_{\rm ee}$ is the di-electron invariant mass, are used in the QCD background estimate. This choice maximizes the ratio of Z signal to background. The sidebands used to estimate the background contribution within the Z window are defined such that 71 GeV $\leq m_{\rm ee} <$ 81 GeV and 101 GeV $\leq m_{\rm ee} <$ 111 GeV.

The full reweighting procedure is applied to the Z signal region and the two sideband regions independently. Only Z signal events are used in the calculation of the di-EM p_T weights for the Z signal region, and likewise only the events within a given sideband region are used in the calculation of the weights for that region. Assuming a constant $t\bar{t}$ background shape, the resulting reweighted sideband $\not\!\!E_T$ distributions are added together and subtracted from the reweighted Z signal $\not\!\!E_T$ distribution. The sideband subtracted Z signal $\not\!\!E_T$ distribution is then normalized as discussed in Secs. 1.1.1 and 1.1.3. The statistical and reweighting error from the sideband regions is propagated to the error on the final ee QCD $\not\!\!E_T$ estimate.

The di-EM p_T weights for the two ee sideband regions are shown in figure **??**. The overall scale of the weights, as well as the trend with di-EM p_T, is similar for the two regions (except at high di-EM p_T, where the statistics are poor anyway). Figure 1.9 shows the $\not\!\!E_T$ spectra for the two sideband regions and the Z signal region after subtraction. The shapes of the spectra indicate that the high-$\not\!\!E_T$ $t\bar{t}$ tail, present in the sideband distributions, was successfully subtracted from the Z signal distribution.

The ee (81 GeV $\leq m_{\rm ee} <$ 101 GeV), $\not f\not f$, and $\gamma\gamma$ di-EM p_T spectra for events with 0, 1, or $\geq$ 2 jets (as in Table **??**) are shown in Figure 1.10. Broad humps in the $\not f\not f$ and $\gamma\gamma$ spectra are due to kinematic ΔR and p_T turn-ons that are suppressed in the ee sample due to the invariant mass cut. Figure 1.11 shows the weights applied to

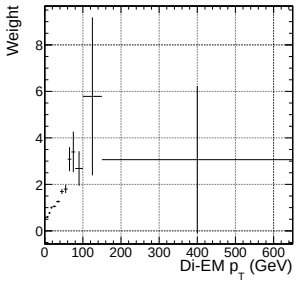

(a) 71 GeV $\leq m_{ee} <$ 81 GeV, 0 jets.

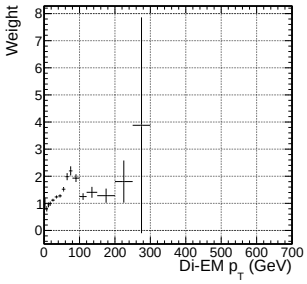

(b) 71 GeV $\leq m_{ee} <$ 81 GeV, 1 jet.

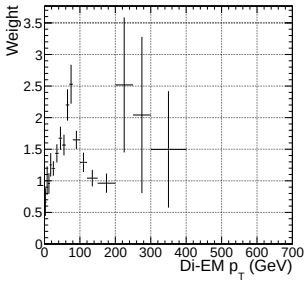

(c) 71 GeV $\leq m_{ee} <$ 81 GeV, $\geq$ 2 jets.

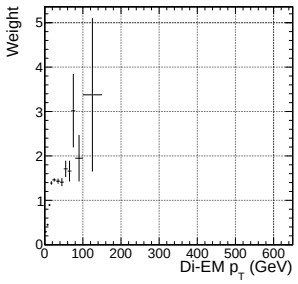

(d) 101 GeV $\leq m_{ee} <$ 111 GeV, 0 jets.

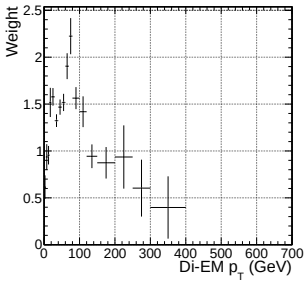

(e) 101 GeV $\leq m_{ee} <$ 111 GeV, 1 jet.

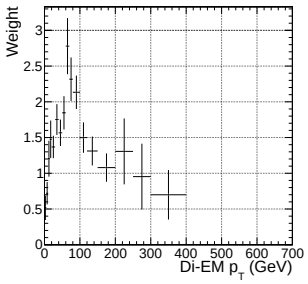

(f) 101 GeV $\leq m_{ee} <$ 111 GeV, $\geq$ 2 jets.

Figure 1.8: *ee* sideband di-EM p_T weights for events with 0, 1, or $\geq$ 2 jets (as in Table **??**). Errors are statistical only.

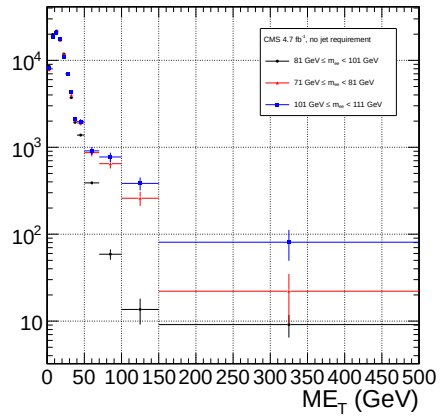

Figure 1.9: $\not\!\!E_T$ spectra of the *ee* sample for 71 GeV $\leq m_{ee} <$ 81 GeV (red triangles), 81 GeV $\leq m_{ee} <$ 101 GeV (black circles), and 101 GeV $\leq m_{ee} <$ 111 GeV (blue squares). The two sideband distributions (red and blue) are normalized to the area of the Z signal distribution (black). Errors on the sideband distributions are statistical only, while the error on the Z signal distribution includes statistical, reweighting, and normalization error (see Sec. 1.3).

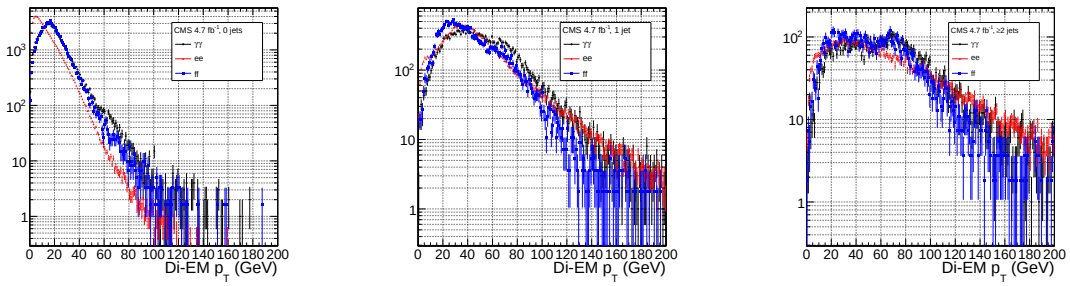

(a) 0 jets. (b) 1 jet. (c) ≥ 2 jets.

Figure 1.10: ee (81 GeV $\leq m_{\mathrm{ee}} <$ 101 GeV) (red triangles), ff (blue squares), and $\gamma\gamma$ (black circles) di-EM p_T spectra for events with 0, 1, or ≥ 2 jets (as in Table **??**). Errors are statistical only. **Zoom out the x-axis to show the full tail out to 500 GeV?**

the ee (81 GeV $\leq m_{\mathrm{ee}} <$ 101 GeV) and ff $\not\!\!E_T$ spectra as a function of di-EM p_T and number of jets per event.

1.1.3 Normalization

After reweighting, the $\not\!\!E_T$ distributions of the QCD control samples are normalized to the $\not\!\!E_T < 20$ GeV region of the candidate $\gamma\gamma$ $\not\!\!E_T$ spectrum, where signal contamination is low. The normalization factor is $(N_{\gamma\gamma}^{\not\!\!E_T<20\mathrm{GeV}} - N_{e\gamma}^{\not\!\!E_T<20\mathrm{GeV}})/N_{\mathrm{control}}^{\not\!\!E_T<20\mathrm{GeV}}$, where $N_{e\gamma}^{\not\!\!E_T<20\mathrm{GeV}}$ is the expected number of electroweak background events with $\not\!\!E_T < 20$ GeV (discussed in Section 1.2).

1.2 Modeling the Electroweak Background

$W\gamma$, W + jet, and $t\bar{t}$ processes in which the W decay electron is misidentified as a photon (due to a failure to properly associate a pixel seed to the electron candidate) can contribute significantly to the high-$\not\!\!E_T$ tail of the $\gamma\gamma$ $\not\!\!E_T$ spectrum. To estimate this background, the $e\gamma$ sample, which is enriched in $W \to e\nu$ decays, is scaled by $f_{e\to\gamma}/(1-f_{e\to\gamma})$, where $f_{e\to\gamma}$ is the rate at which electrons are misidentified as photons. The derivation of this scaling factor comes from the two equations

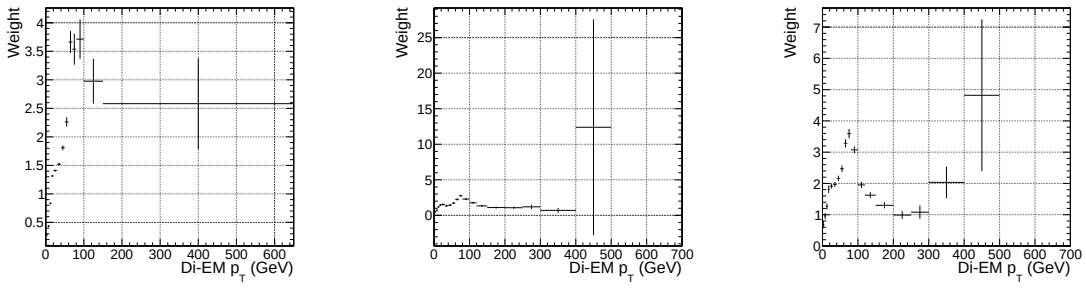

(a) ee, 0 jets. (b) ee, 1 jet. (c) ee, ≥ 2 jets.

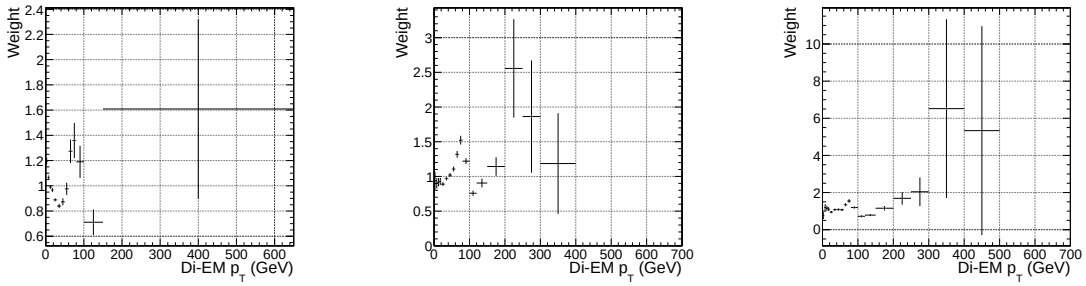

(d) $\not{f}\not{f}$, 0 jets. (e) $\not{f}\not{f}$, 1 jet. (f) $\not{f}\not{f}$, ≥ 2 jets.

Figure 1.11: ee (81 GeV $\leq m_{\mathrm{ee}} <$ 101 GeV) and $\not{f}\not{f}$ di-EM p_T weights for events with 0, 1, or ≥ 2 jets (as in Table **??**). Errors are statistical only. **Zoom in the x-axis to hide large weights with large statistical errors?**

$$N^W_{e\gamma} = f_{e\to e} N_W \tag{1.2}$$

$$N^W_{\gamma\gamma} = (1 - f_{e\to e}) N_W \tag{1.3}$$

where $N^W_{e\gamma}$ is the number of W events in the $e\gamma$ sample in which the electron was correctly identified, $f_{e\to e}$ is the probability to correctly identify an electron, N_W is the true number of triggered $W \to e\nu$ events, and $N^W_{\gamma\gamma}$ is the number of W events in the $\gamma\gamma$ sample in which the electron was misidentified as a photon. The contribution from $Z \to ee$ can be neglected (i.e. $f_{e\to\gamma}$ is small and the Z contribution involves $f^2_{e\to\gamma}$, since both electrons have to be misidentified). Since $f_{e\to e} = 1 - f_{e\to\gamma}$, solving for $N^W_{\gamma\gamma}$ gives

$$N^W_{\gamma\gamma} = \frac{f_{e\to\gamma}}{1 - f_{e\to\gamma}} N^W_{e\gamma} \tag{1.4}$$

$f_{e\to\gamma}$ is measured by fitting the Z peaks in the ee and $e\gamma$ samples. The number of Z events fitted in the ee and $e\gamma$ samples, respectively, is given by

$$N^Z_{ee} = (1 - f_{e\to\gamma})^2 N_Z \tag{1.5}$$

$$N^Z_{e\gamma} = 2 f_{e\to\gamma}(1 - f_{e\to\gamma}) N_Z \tag{1.6}$$

where N_Z is the true number of triggered $Z \to ee$ events. Solving for $f_{e\to\gamma}$ gives

$$f_{e\to\gamma} = \frac{N^Z_{e\gamma}}{2N^Z_{ee} + N^Z_{e\gamma}} \tag{1.7}$$

A Crystal Ball function is used to model the Z signal shape in both the ee and $e\gamma$ samples, while an exponential convoluted with an error function ("RooCMSShape", see Sec. **??**) is used to model the background shape. The fixed fit parameters are identical for the two samples, but the other parameters are allowed to float independently. Table 1.3 shows the values and ranges of the fixed and floating fit parameters, respectively. **Edit this to reflect the actual study once done.**

Fits to the ee and $e\gamma$ invariant mass spectra are shown in Figure **??**. **Make these plots.** Figure **??** indicates that the dependence of $f_{e\to\gamma}$ on the electron p_T and η is small. Applying a p_T- and η-dependent misidentification rate (with p_T and η binned as in Fig. **??**) makes only a **XXX%** difference in the final electroweak background estimate with respect to a constant rate derived from all ee and $e\gamma$ events, which is well within the statistical and systematic errors. **Prove this statement.** Therefore,

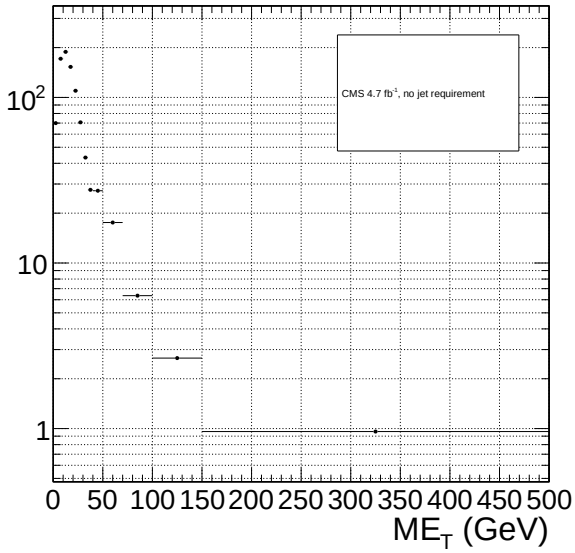

Figure 1.12: $\not\!\!E_T$ spectrum of the $e\gamma$ sample after scaling by $f_{e\to\gamma}$. The total error on $f_{e\to\gamma}$ is propagated to the total error on the electroweak background estimate. **How to properly treat the error when the same events are used in the $f_{e\to\gamma}$ calculation and in the $e\gamma$ sample? Replace with figure using latest $f_{e\to\gamma}$, and include error bars.**

the constant rate is used in the final electroweak background estimate. **Check this statement.**

The signal and background shape assumptions are the main sources of systematic error on $f_{e\to\gamma}$. To assess the magnitude of this error, $f_{e\to\gamma}$ is recalculated using both linear and quadratic background shapes, and with a Crystal Ball + generated Z signal shape (as used in Sec. **??**). The largest difference from the nominal shape is taken as the error. **Check that this is how it was done, and do it yourself. Also check the misidentification rate in MC with varied tracker radiation lengths to see if there is a dependence on the tracker density.**

Using the integrals of the Z fits shown in Fig. **??**, Eq. 1.7, and the shape systematic discussed above, $f_{e\to\gamma}$ is calculated to be $0.015 \pm 0.002(\text{stat.}) \pm 0.005(\text{syst.})$. **Replace with your calculated number.** The scaled $e\gamma$ MET distribution is shown in Figure 1.12.

In the 36 pb^{-1} version of this analysis [**?**], it was shown that the ee sample could

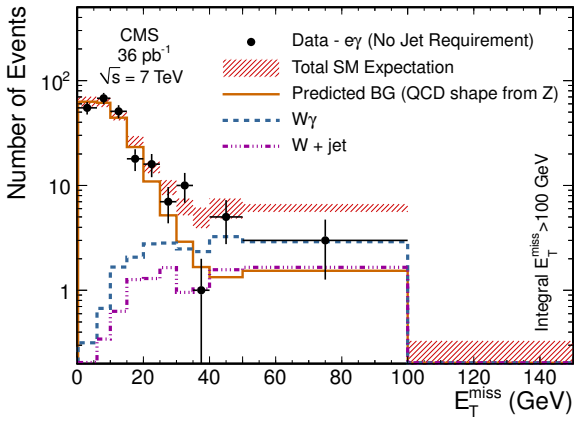

Figure 1.13: $\not\!\!E_T$ spectrum of the $e\gamma$ sample in 35 pb^{-1} of 2010 LHC data scaled by the 2010 measured $f_{e\to\gamma}$ (black dots), QCD and real Z predicted background from the 2010 ee sample (solid orange line), MC W + jet estimate (dash-dotted purple line), and MC $W\gamma$ estimate (dashed blue line). The total $e\gamma$ prediction (red band) is the sum of the ee, W + jet, and $W\gamma$ predictions. Reprinted from Fig. 2 of ref. [**?**].

accurately predict the QCD and real Z contribution to the $e\gamma$ sample at low $\not\!\!E_T$, and that the expectation from $W \to e\nu$ MC accounted for the remaining W contribution at high $\not\!\!E_T$. A plot of the $\not\!\!E_T$ distributions of the 2010 $e\gamma$ sample and the predicted components is shown in Figure 1.13. **Repeat for current selection?** This exercise helps to validate both the QCD and electroweak background prediction methods.

1.3 Systematic Errors

1.3.1 Jet Energy Scale Uncertainty

The dijet p_T reweighting method utilizes jets corrected for imperfect calorimeter response (see Sec. **??** for a description of the jet reconstruction and correction procedure). Since the applied jet energy scale (JES) factor has an error associated to it due to the limitations of the JES derivation ([**?**] and Sec. **??**), this uncertainty must be propagated to the uncertainty on the dijet p_T weights.

The JES contribution to the dijet p_T weights is estimated by performing 1000 pseudo-experiments on each of the $\gamma\gamma$ and ff samples. For the purpose of estimating

the JES error, the results of the true experiment may be thought of as a set of measurements:

- The set of **uncorrected jet 4-vectors** corresponding to the **leading EM object** in the $\gamma\gamma$ sample $\left\{ \mathrm{p}_{\mathrm{j1}}^{\mu 1}, \mathrm{p}_{\mathrm{j1}}^{\mu 2}, ..., \mathrm{p}_{\mathrm{j1}}^{\mu \mathrm{N}_{\gamma\gamma}} \right\}$
- The set of **uncorrected jet 4-vectors** corresponding to the **trailing EM object** in the $\gamma\gamma$ sample $\left\{ \mathrm{p}_{\mathrm{j2}}^{\mu 1}, \mathrm{p}_{\mathrm{j2}}^{\mu 2}, ..., \mathrm{p}_{\mathrm{j2}}^{\mu \mathrm{N}_{\gamma\gamma}} \right\}$
- The set of **JES** accompanying the uncorrected jet 4-vectors corresponding to the **leading EM object** in the $\gamma\gamma$ sample $\left\{ \mathrm{c}_{\mathrm{j1}}^{1}, \mathrm{c}_{\mathrm{j1}}^{2}, ..., \mathrm{c}_{\mathrm{j1}}^{\mathrm{N}_{\gamma\gamma}} \right\}$
- The set of **JES** accompanying the uncorrected jet 4-vectors corresponding to the **trailing EM object** in the $\gamma\gamma$ sample $\left\{ \mathrm{c}_{\mathrm{j2}}^{1}, \mathrm{c}_{\mathrm{j2}}^{2}, ..., \mathrm{c}_{\mathrm{j2}}^{\mathrm{N}_{\gamma\gamma}} \right\}$
- The set of **JES uncertainties** accompanying the uncorrected jet 4-vectors corresponding to the **leading EM object** in the $\gamma\gamma$ sample $\left\{ \sigma_{\mathrm{cj1}}^{1}, \sigma_{\mathrm{cj1}}^{2}, ..., \sigma_{\mathrm{cj1}}^{\mathrm{N}_{\gamma\gamma}} \right\}$
- The set of **JES uncertainties** accompanying the uncorrected jet 4-vectors corresponding to the **trailing EM object** in the $\gamma\gamma$ sample $\left\{ \sigma_{\mathrm{cj2}}^{1}, \sigma_{\mathrm{cj2}}^{2}, ..., \sigma_{\mathrm{cj2}}^{\mathrm{N}_{\gamma\gamma}} \right\}$
- The set of **uncorrected jet 4-vectors** corresponding to the **leading EM object** in the ff sample $\left\{ \mathrm{p}_{\mathrm{j1}}^{\mu 1}, \mathrm{p}_{\mathrm{j1}}^{\mu 2}, ..., \mathrm{p}_{\mathrm{j1}}^{\mu \mathrm{N}_{\mathrm{ff}}} \right\}$
- The set of **uncorrected jet 4-vectors** corresponding to the **trailing EM object** in the ff sample $\left\{ \mathrm{p}_{\mathrm{j2}}^{\mu 1}, \mathrm{p}_{\mathrm{j2}}^{\mu 2}, ..., \mathrm{p}_{\mathrm{j2}}^{\mu \mathrm{N}_{\mathrm{ff}}} \right\}$
- The set of **JES** accompanying the uncorrected jet 4-vectors corresponding to the **leading EM object** in the ff sample $\left\{ \mathrm{c}_{\mathrm{j1}}^{1}, \mathrm{c}_{\mathrm{j1}}^{2}, ..., \mathrm{c}_{\mathrm{j1}}^{\mathrm{N}_{\mathrm{ff}}} \right\}$
- The set of **JES** accompanying the uncorrected jet 4-vectors corresponding to the **trailing EM object** in the ff sample $\left\{ \mathrm{c}_{\mathrm{j2}}^{1}, \mathrm{c}_{\mathrm{j2}}^{2}, ..., \mathrm{c}_{\mathrm{j2}}^{\mathrm{N}_{\mathrm{ff}}} \right\}$

- The set of **JES uncertainties** accompanying the uncorrected jet 4-vectors corresponding to the **leading EM object** in the ff sample $\left\{\sigma^{1}_{\mathrm{cj1}}, \sigma^{2}_{\mathrm{cj1}}, ..., \sigma^{\mathrm{N_{ff}}}_{\mathrm{cj1}}\right\}$
- The set of **JES uncertainties** accompanying the uncorrected jet 4-vectors corresponding to the **trailing EM object** in the ff sample $\left\{\sigma^{1}_{\mathrm{cj2}}, \sigma^{2}_{\mathrm{cj2}}, ..., \sigma^{\mathrm{N_{ff}}}_{\mathrm{cj2}}\right\}$

From these measurements, the $\gamma\gamma$ and ff dijet $\mathrm{p_T}$ spectra and the resulting ff dijet weights can be calculated. In each of the 1000 pseudo-experiments, a new set of JES factors is generated according to the measured JES uncertainties, and new dijet $\mathrm{p_T}$ spectra and weights are subsequently calculated. The spread of the 1000 weights (binned in dijet $\mathrm{p_T}$) is taken as the error due to JES uncertainty. The total error on the weights is the quadrature sum of the JES error and the statistical error, and is propagated to the error on the final $\not\!\!E_T$ measurement via a similar pseudo-experiment procedure described in Sec. 1.3.2.[2]

If the JES uncertainty were to cause the jet energy to be reconstructed below the 20 GeV ntuple cut, there could be a small error or bias in the $\not\!\!E_T$ introduced due to EM-matched jets falling below the matching threshold. The percentage of jets lost due to jet $\mathrm{E_T}$ matching threshold has been checked in data, and found to be X% (X% of events). Furthermore, the trailing EM $\mathrm{E_T}$ cut is 25 GeV/c, implying that the JES would have to be mis-measured by at least 20% to fall below the jet matching threshold. Since the typical JES uncertainty is no more than 5%, a mis-measurement of this type is a 4σ event and should occur in only 0.1% of cases. As expected, this effect is negligible, as shown in Figure X.

1.4 Results

[2]The $\not\!\!E_T$ is uncorrected and therefore its central value per event is unaffected by a change in the JES.

Table 1.3: Parameter values for the signal and background PDFs for the ee and $e\gamma$ samples. When a bracketed range is given, the parameter is allowed to float within that range. When a constant is given, the parameter is fixed to that constant. **Edit this to reflect the actual study once done.**

	Crystal Ball fit parameters				RooCMSShape fit parameters			
PDF	μ	σ	α	n	μ	α	β	γ
ee signal	[-1.0, 1.0]	[1.0, 3.0]	0.87	97.0	N/A	N/A	N/A	N/A
$e\gamma$ signal	[-1.0, 1.0]	[1.0, 3.0]	0.73	134.9	N/A	N/A	N/A	N/A
ee background	N/A	N/A	N/A	N/A	65.0	61.949	0.04750	0.01908
$e\gamma$ background	N/A	N/A	N/A	N/A	α	[50.0, 100.0]	0.065	0.048